

Violation of Stokes-Einstein and Stokes-Einstein-Debye relations in a supercooled polymer melt

Jalim Singh and Prasanth P. Jose*

School of Basic Sciences, Indian Institute of Technology Mandi, Kamand, Himachal Pradesh 175005, India

Molecular dynamics simulations are performed on a model linear polymer melt to look at the violations of Stokes-Einstein (SE) and Stokes-Einstein-Debye (SED) relations near the mode coupling theory transition temperature T_c at three (one higher and two lower) densities. At low temperatures, both lower density systems form stable bi-continuous phases whereas the higher density system is homogeneous. We show that monomer density relaxation exhibits SE violation for all three densities, whereas molecular density relaxation shows weak violation of the SE relation near T_c in both lower density systems. This study identifies disparity in monomer mobility and observation of jump like motion in the typical monomer trajectories resulting in the SE violations. In addition to the SE violation, weak SED violation is observed in bi-continuous phases of lower densities in the supercooled state. Both lower density systems also show decoupling of translational and rotational dynamics in this polymer system.

I. INTRODUCTION

Simple liquids show coupling of translational diffusion coefficient D and viscosity η through the SE relation [1–3]

$$D = \frac{k_B T}{c\pi\eta r}, \quad (1)$$

where k_B is the Boltzmann constant, r is effective radius of a Brownian particle immersed in the fluid. The constant $c = 4$ and 6 in Eq. (1) are respectively for slip and stick boundary conditions. Eq. (1) can be written as $D\eta/T = \text{constant}$ that obeys in the liquids at high temperatures. A calculation of η of a system is computationally expensive in the supercooled liquids due to the large fluctuations in their stress autocorrelation functions [4]. Therefore, instead of viscosity η , the relaxation time τ is computed in the simulations of glass-forming liquids (GFLs) with the approximation $\tau \propto \eta/T$ [5–9]. Deviations from $D\tau = \text{constant}$ are considered as the SE violations due to the decoupling in D and τ . Violation of the SE relation has been observed in simulations [5, 10–13] and experiments [14–16] of several supercooled GFLs. Earlier studies show that a possible reason for the violation of the SE relation is dynamical heterogeneity (DH) in the supercooled liquids [14, 17, 18]. There is a consensus among the glass community that glassy systems lose homogeneity in the dynamics due to the presence of mobile (fast moving) and immobile (caged) particles [19], noticeably in fragile GFLs [14]. The mobile particles move faster than the average motion, while immobile particles move slowly in the system. This difference in the motion of the particles in different regions of the system results in the DH [14, 17–22].

Near the glass transition, D is dominated by the mobile particles, whereas τ is dictated by the immobile particles

(as majority of the particles are caged). Increment in τ is not accompanied by the decrement in D due to different mobilities in the system, causing a decoupling in D and τ , which results in the breakdown of the SE relation. Many researchers have argued that the hopping of particles from the cages formed by their neighbors has a role in the violation of the SE relation in the supercooled and glassy state of the GFLs [23–25]. Kumar *et al.* [26] show that the SE relation violates due to the presence of mobile particles, whereas immobile particles obey it, in the supercooled state of a hard sphere liquid. However, few recent studies show that both mobile and immobile particles violate the SE relation [10, 12].

In molecular GFLs, system shows violation of SED relation defined for the rotational degrees of freedom. Similar to Eq. (1), the rotational correlation time τ_l of l th order Legendre polynomial is related to the viscosity η , which is known as the SED relation for the molecules [27–29]

$$\frac{1}{\tau_l} = \frac{l(l+1)k_B T}{6\eta V_h}, \quad (2)$$

where V_h is the hydrodynamic volume of a molecule. The coupling between viscosity η and rotational correlation time τ_l of molecular liquids holds the SED relation at high temperatures, whereas it violates in the supercooled liquids and glasses [15, 30, 31]. The hydrodynamic volume V_h is related to the radius of gyration R_g of polymers as $V_h \propto R_g^3$, which shows a weak temperature dependence for this system, therefore, $V_h \approx \text{constant}$ [32]. Using this approximation, Eq. (2), and Eq. (1) suggest that $D\tau_l = \text{constant}$ in molecular liquids at high temperatures [29], which means that the translational molecular diffusion D is coupled to the rotational relaxation time τ_l of the molecules. However, Translation-rotation decoupling is observed in many GFLs [33, 34]. Michele *et al.* [35, 36] relate the translational and rotational jump dynamics to the violation of SE and SED relations in a diatomic molecular liquid and rigid dumbbell molecules.

Extending such studies (performed on binary mixtures

* prasanth@iitmandi.ac.in

and dumbbells) to polymers is a daunting task due to complexity of the system. Identification of jump-like motions are reported in the continuous time random walk simulation of Helfrich *et al.* [37] with special definition of the jumps in a supercooled short chain melt. Another study by Pousi *et al.* [11, 38] argued that picosecond dynamics of the caged particles corresponding to the short time (β -relaxation), is related to the violation of SE relation in supercooled linear polymers. A very recent study shows that the violation of SE relation is related to the structural changes in the supercooled linear polymer melt [39]. Therefore, due to the molecular complexity it is strenuous to examine the SE and SED violation in polymer liquids and to identify the possible reason compared to the simulation studies of atomic GFLs. This study attempts a direct identification of SE and SED violations in a simple polymer model that is known to undergo glass transition and relates it to the known reasons that are manifestations of DH in atomic GFLs.

Polymers are extended systems that relax by collective rearrangements of monomers in a chain and neighbouring chains. Therefore, identification of the mobile and immobile particles is expected to be easier in low density where there is more free-space available at lower temperatures. Polymer systems with attractive interactions in the lower density form bi-continuous phases at lower temperatures with cavities. On the surface of these cavities there is free space available for chains leading to large variation in mobilities, which can show direct evidence of SE and SED violations and their possible microscopic origins. In this study, we examine the violations of the SE and SED relations in a linear polymer melt system at number densities $\rho = 1.0$ [40], 0.85 [41], and 0.7, which we call as one higher and two lower (relatively) density systems in the grid of high to low temperatures ($T = 2.0 - 0.36$), near their respective T_c , *i.e.*, 0.36 for higher density, and 0.4 for lower densities. Both lower density systems are quenched beyond the spinodal limit of stability, which phase separate via spinodal decomposition [42] resulting in stable bi-continuous phases with long equilibration. Details of non-equilibrium dynamics of cavity formation are studied in many earlier studies [43–47]. In this study, monomer relaxation shows SE violation in all three systems: both lower density systems show pronounced violation that is attributed to the enhanced disparity in the motion of the monomers that arises due to surface of the cavities. A pronounced violation of SE relation is due to both the mobile and immobile particles, which agrees with the earlier studies on violation of SE and SED relations in atomic model GFLs [10, 12]. The SED relation is obeyed in the higher density system, whereas it is weakly violated in both lower density systems.

The rest of the manuscript is organized as follows: Sec. II gives the details of the simulations. Results are presented in subsections of section III. Subsec. III A present stability analysis of the bi-continuous phase. Study of polymer relaxation and diffusion is presented in Subsec. III B, SE violations are discussed in Subsec. III C, the

distribution of particles mobility and jump like motions are presented in Subsec. III D, and violation of SED and orientational diffusion is detailed in Subsec. III E. Sec. IV present conclusions and summary of this paper.

II. SIMULATION DETAILS

We simulate a system of $N_c = 1000$ fully flexible-linear polymer chains, consisting of $n = 10$ beads (number of monomers $N = 10000$) in each chain. The system is simulated at the constant number density of monomers $\rho = 0.7, 0.85$, and 1.0. The inter-particle interactions are modelled by the truncated and shifted Lennard-Jones (LJ) potential, defined in terms of the particle diameter, σ and the depth of the potential well, ϵ as

$$V_{LJ}(r) = 4\epsilon \left[\left(\frac{\sigma}{r} \right)^{12} - \left(\frac{\sigma}{r} \right)^6 \right] - V_{LJ}(r_c). \quad (3)$$

Here, the LJ potential cut-off is $r_c = 2 \times 2^{1/6}\sigma$. The bond connectivity between consecutive monomers along a chain is modelled by the LJ and finitely extensible non-linear elastic (FENE) potentials [41, 48]; the FENE potential is given in terms of R_0 , the maximum displacement between a pair of consecutive monomers, and the elastic constant k_0 as

$$V_{FENE}(r) = \begin{cases} -\frac{1}{2}k_0R_0^2 \ln \left(1 - \frac{r^2}{R_0^2} \right) - E_b & 0 < r < R_0 \\ \infty & r \geq R_0, \end{cases} \quad (4)$$

where $k_0 = 30\epsilon/\sigma^2$ and $R_0 = 1.5\sigma$. The equations of motion are integrated using the velocity Verlet algorithm [49] with time step $\Delta t = 0.002$ for $\rho = 0.85$, and $\Delta t = 0.0001$ for $\rho = 1.0$ and 0.7 system. We prepare the linear polymer melt at temperature $T = 8.0$ for the respective density, in the constant NVE ensemble. The equilibrated configurations of the $T = 8.0$ is used as an initial configuration for the temperatures $T = 2.0 - 0.36$. Long simulation time before the production runs ensures fluctuation of the system around the average target temperature during the data collection in constant NVE ensemble and follow a criterion of the time required for the relaxation of end-to-end vector below 10% of its initial value at all temperatures [37]. All the quantities presented in this work are in LJ units, *i.e.*, length is expressed in terms of the bead diameter σ , the number density as σ^{-3} , the temperature as ϵ/k_B , and the time as $\sqrt{m\sigma^2/\epsilon}$.

III. RESULTS AND DISCUSSIONS

A. Steady state density relaxation in a bi-continuous phase

State points corresponding to decreasing order of temperatures in both lower density systems show bi-continuous phases (see Fig. 8 and Fig. S1 of supplementary material (SM) [50]), which is a mixture of gas and

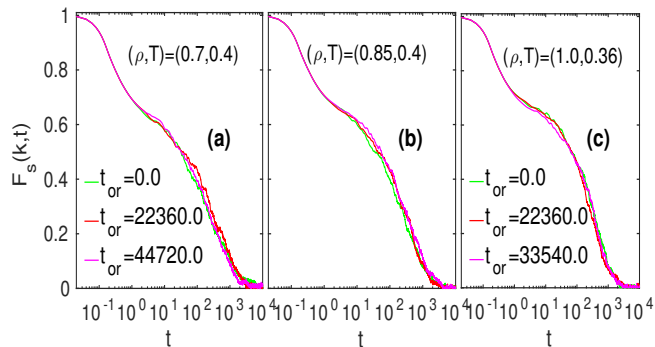


Figure 1. Incoherent intermediate scattering function, $F_s(k, t)$ is calculated at different time origins of the low temperatures for $\rho = 1.0, 0.85, 0.7$. The legend in (b) is same as in (c).

liquid at intermediate temperatures, *e.g.*, $T = 0.7$ for $\rho = 0.85$ and $T = 1.0$ for $\rho = 0.7$. However, the system shows bi-continuous phase, consisting of dilute gas and the supercooled liquid at lower temperatures. In moderately supercooled state, system attains its steady state where the cavities are stable, whereas the cavities at liquid-gas phase coexistence move, and the system attains density relaxation. Before presenting the glass transition studies, we look at the single particle and collective density relaxation to ensure an absence of aging in the system. Studies on aging near the glass transition compare time origin dependent density relaxation using incoherent intermediate scattering function $F_s(k, t)$ [51], which show different relaxation time for different time origins. Therefore, we look into the relaxation of density fluctuations in $F_s(k, t)$ [1] at time origins longer than the α -relaxation time (presented later in this paper), which is defined as

$$F_s(k, t) = \frac{1}{N} \langle \rho_{\mathbf{k}}^s(t) \rho_{-\mathbf{k}}^s(0) \rangle, \quad (5)$$

where $\rho_{\mathbf{k}}^s(t) = \exp(-i\mathbf{k} \cdot \mathbf{r}_i(t))$. Here, k is the wavenumber and \mathbf{r}_i is the position of the i th particle. The $F_s(k, t)$ is calculated at a wavenumber k that corresponds to the first peak of static structure factor $S(k)$, which is shown in Fig. 1; $k = 6.9$ for $\rho = 0.85$ and $k = 7.1$ for $\rho = 0.7$ and $\rho = 1.0$. The α -relaxation time of the monomers $\tau_\alpha = \int_0^\infty F_s(k, t) dt$ gives the relaxation time of the transient cages formed by their neighbouring particles. The time difference between two time origins is chosen to be greater than the τ_α (see Fig. S3 of SM [50] for τ_α) to look at the average density relaxation of the monomers in that time window. The $F_s(k, t)$ of all three densities at the lowest temperatures (see Fig. 1(a-c)) does not show any systematic variation in the nature of density relaxation with time at different time origins of the correlation, therefore, they are independent of the time origin. The minor difference due to fluctuation in the tail of $F_s(k, t)$ in lower densities is similar to that at the higher density.

Collective relaxation dynamics of the bi-continuous

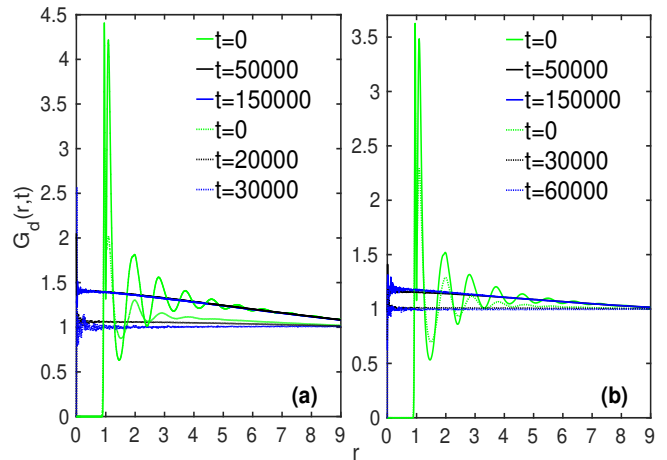


Figure 2. Distinct part of van-Hove correlation function scaled with the density is plotted in (a) $\rho = 0.7$ and (b) $\rho = 0.85$. Solid lines in (a) and (b) are at $T = 0.4$. Dotted lines in (a) are at $T = 1.0$, while in (b) are at $T = 0.7$.

system is examined by distinct part of van-Hove correlation function, $G_d(r, t)$ [1],

$$G_d(\mathbf{r}, t) = \frac{1}{N} \left\langle \sum_{i=1}^N \sum_{j=i+1}^N \delta(\mathbf{r} + \mathbf{r}_i(0) - \mathbf{r}_j(t)) \right\rangle, \quad (6)$$

that shows collective structural relaxation in different coordination shells with respect to a reference particle at $t = 0$. Fig. 2 shows the $G_d(r, t)/\rho$ of the monomers at one low and one high temperature of both lower densities at different times starting from $t = 0$. At $t = 0$, $G_d(r, 0)/\rho = g(r)$ is showing oscillations above 1.0, which is due to the phase separation in the system. The neighbouring particles around a tagged particle move as time progresses from their initial positions, leading to decay of the $G_d(r, t)$ to 1.0 as in a homogeneous system ($T = 1.0$). However, $G_d(r, t)/\rho$ remains above 1.0 for both lower density systems that form bi-continuous phases at low temperatures even at longest time scale in this study. Interestingly, Fig. 2 shows that the $G_d(r, t)$ of both lower densities coincides at times $t = 5 \times 10^3$ and $t = 1.5 \times 10^5$, which shows that the shape and location of the cavities are stable and do not change within our simulation time in the moderately supercooled state. It is now interesting to look at the slow polymer relaxation dynamics in the higher and both lower density systems as temperature reduces.

B. Polymer relaxation and diffusion

The self diffusion coefficient D of the monomers can be calculated using their mean-squared displacement (MSD) as $D = \lim_{t \rightarrow \infty} \langle (\mathbf{r}(t) - \mathbf{r}(0))^2 \rangle / 6t$. Near the glass transition of unentangled polymer melts, the monomer MSD takes longer time to attain diffusive regime due to the chain

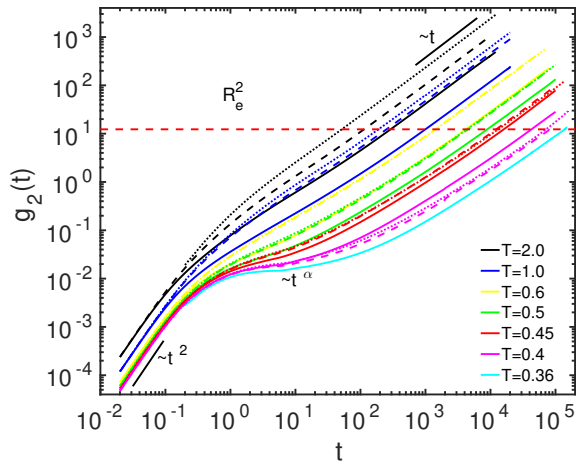


Figure 3. Center of mass MSD of chains, $g_2(t)$ is plotted against time t . Solid, dashed, and dotted lines are corresponding to the density $\rho = 1.0, 0.85,$ and 0.7 respectively. At temperatures $T = 2.0-0.45$, $g_2(t)$ of the higher density system is slower than both lower density systems. However, both lower density systems show slow molecular movement than the higher density system from $T = 0.4$ to below. At low temperatures ($T = 0.5-0.4$), the sub-diffusive regime ($g_2(t) \sim t^\alpha$) becomes pronounced due to the molecular cages, which is separated by the short time ballistic ($g_2(t) \sim t^2$) and long time diffusive ($g_2(t) \sim t$) regimes.

connectivity [52]. Therefore, the monomer MSD shows a power law dependency as $\langle(\mathbf{r}(t) - \mathbf{r}(0))^2\rangle = 6Dt^{0.63}$, before the starting of its diffusion [52]. However, the MSD of the polymer molecules (center of mass) shows the diffusion at early times, though they perform slow motion at short time and coincides with the monomer MSD at the long times $t \simeq 10^6$ [52, 53]. Therefore, we calculate the self diffusion coefficient from the center of mass MSD, as both of them are identical at long times. We calculate the self diffusion coefficient D when the exponent $\alpha = 1.0$ in the relation $g_2(t) = \langle(\mathbf{r}_{cm}(t) - \mathbf{r}_{cm}(0))^2\rangle = 6Dt^\alpha$, where $t > 10^5$ in the LJ units at the lowest temperatures (see Fig. 3). At this time scale, the molecular MSD also crosses the average squared end-to-end distance, *i.e.*, $g_2(t) > R_e^2$, which is shown by the red line $g_2(t) = R_e^2$ in Fig. 3. Using the approximation $\tau \propto \eta/T$ (as discussed above), the fractional SE relation becomes $D \sim \tau^{-\xi}$ ($0 < \xi < 1$), which shows that the diffusion coefficient and relaxation time (or viscosity) decouple from the usual SE relation (Eq. 1). This is also reported in various earlier studies of supercooled liquids and glasses [10, 13, 18, 26].

Earlier studies argued that one of the possible reason for the violation of SE relation is the caging and hopping of the particles in the glassy state of the GFLs, which results into the spatially heterogeneous dynamics [14, 17, 18, 23–25]. The slow down of density relaxation due to transient caging, and increase in the relaxation time with reduction in the temperature, can be examined from the $F_s(k, t)$. Fig. 4(a) shows $F_s(k, t)$ of monomers at wave vector $k = 6.9$ for $\rho = 0.85$, $k = 7.1$ for $\rho = 0.7$, and $\rho = 1.0$ at

Density	MCT fitting		VFT fitting	
	T_c	Exponent γ	T_0	Fragility parameter A
$\rho = 1.0$	0.33	1.54	0.22	4.4
$\rho = 0.85$	0.4	1.65	0.3	2.34
$\rho = 0.7$	0.4	1.56	0.3	2.58

Table I. Fitting parameters for MCT and VFT relations at three densities: MCT transition temperature T_c , MCT exponent γ , dynamic divergence temperature T_0 , and fragility parameter A . T_c and T_0 are lower for the higher density system and fragility is smaller as fragility $\propto 1/A$ [54].

all the temperatures. As temperature reduces, a hump appears in $F_s(k, t)$ from temperature $T = 0.5$ for both lower densities, whereas it starts from $T = 0.6$ for the higher density system. The appearance of a hump in the $F_s(k, t)$ of all three systems indicates a commencement of monomer caging that enhances their α -relaxation time. It is evident from the Fig. 4(a) that the $F_s(k, t)$ of both lower density systems shows slower relaxation dynamics than that of the higher density system at $T = 0.4$, thus show a crossover. The heterogeneity in the relaxation is quantified from fitting of the tail of $F_s(k, t)$ with empirical Kohlrausch-Williams-Watts (KWW) function of the form $f(t)^{KWW} \propto \exp[-(t/\tau)^\beta]$ below temperature $T = 2.0$ with the value of exponent β varies from 0.92 to 0.59 for $\rho = 0.85$, 0.94 to 0.55 for $\rho = 0.7$, and from 0.85 to 0.72 for the higher density system. This shows that lower densities exhibit more heterogeneous dynamics, which is a result of heterogeneous density distribution due to the formation of the cavities (see nearest neighbour distribution in Fig. S1 of SM [50]). The characteristic temperatures of the glass transition are determined from the plot of τ_α against T (see Fig. S3 of SM [50]) by fitting of schematic mode coupling theory (MCT) and Vogel-Fulcher-Tammann (VFT) relations, respectively, as $\tau_\alpha \propto (T - T_c)^{-\gamma}$ and $\tau_\alpha \propto \exp(AT_0/(T - T_0))$. The fitting parameters of these two equations for the density $\rho = 1.0, 0.85,$ and 0.7 are shown in Table I. This fitting shows that the lower density systems are more fragile than the higher density system as their fragility parameter is smaller than the higher density system.

The molecular density relaxation is computed as $F_s^C(k, t) = N_c^{-1} \langle \rho_{\mathbf{k}}^C(t) \rho_{-\mathbf{k}}^C(0) \rangle$, where $\rho_{\mathbf{k}}^C(t) = \exp(-i\mathbf{k} \cdot \mathbf{r}^{cm}(t))$ and $\mathbf{r}^{cm}(t)$ is the position of the center of mass of a polymer molecule at time t . Fig. 4(b) shows that the $F_s^C(k, t)$ of lower and higher density systems are plotted against time t at several temperatures, and the wave vector $k = 2\pi/2R_g \sim 2.1$. Here, R_g is the average radius of gyration of polymer chains in lower and higher density systems that are 1.46 and 1.45. Thus, the diameters are $2R_g = 2.92$ and 2.9 , and we consider $2R_g = 2.9$. The relaxation of density fluctuations of the center of mass shows that the initial fast relaxation found in the $F_s(k, t)$, is insignificant in $F_s^C(k, t)$ because the fluctuations in the density relaxations due to the monomers are

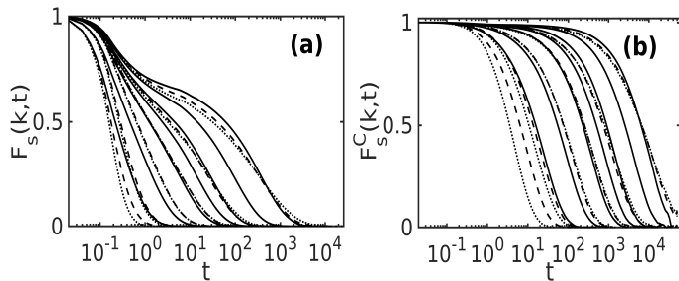


Figure 4. (a) Incoherent scattering function of monomers, (b) Center of mass incoherent scattering function. Solid, dashed, and dotted curves corresponds to the density $\rho = 1.0$, $\rho = 0.85$, and $\rho = 0.7$. In (a) and (b) temperature decreases from left to right.

averaged out. In Fig. 4(b), the $F_s^C(k, t)$ of both lower density systems shows crossover to longer relaxation time in comparison to the higher density system at the same temperature $T = 0.4$; the $F_s^C(k, t)$ of both lower density systems at $T = 0.4$ is comparable to the $F_s^C(k, t)$ of the higher density system at $T = 0.36$. To examine the time scale of the molecular relaxations, we calculate molecular relaxation time $\tau_{2R_g} = \int_0^\infty F_s^C(k, t) dt$, which is higher at high (and intermediate) temperatures for the higher density system compare to the lower density systems. However, in the moderately supercooled regime near T_c there is a crossover similar to the case of monomer density relaxation (see Fig. S6). Now, we look into the violation of SE and SED relations at these state points of the system.

C. Violation of Stokes-Einstein relations

To examine the violation of SE relation, we compute exponent of the power law dependence of diffusion constant on the relaxation time, *i.e.*, $D \sim \tau_\alpha^{-\xi}$ at different densities. Fig. 5 shows that $\xi = 1.0$ for the higher density, whereas $\xi = 1.33$ and 1.21 for $\rho = 0.7$ and 0.85 , respectively, in the temperature range $T = 2.0 - 0.6$. Exponent $\xi > 1$ shows the decoupling of D and τ_α in the normal liquid temperatures, which is also reported in many studies including Refs. [5, 55]. In moderately supercooled regime ($T = 0.5 - 0.36$), the value of $\xi = 0.83$ for the higher density system, and $\xi = 0.73$ and 0.66 for $\rho = 0.85$ and 0.7 , respectively, thus shows decoupling of D and τ_α . The decreasing value of ξ with the density suggests that the decoupling increases with decreasing density. A smaller value of ξ in the supercooled regime of both lower density systems shows the pronounced violation of the SE relation, and in particular, the violation is more pronounced for the lower density $\rho = 0.7$.

Another way of estimating the SE breakdown is the predictors of violation of the SE relation [5–8], *e.g.*, $D\tau_\alpha(T)$. We compute SE ratio as $D\tau_\alpha(T)/D\tau_\alpha(T = 1.0)$, where $D\tau_\alpha$ at temperature $T = 1.0$ is a reference point (see Fig. 6(a)). Fig. 6(a) shows that the SE ratio starts

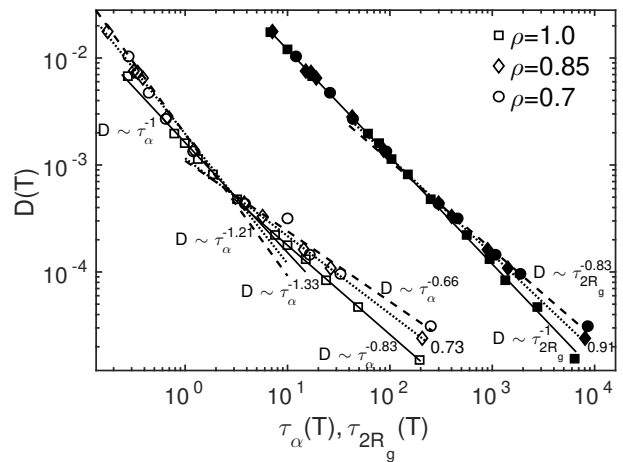


Figure 5. Self diffusion coefficient $D(T)$ is plotted against $\tau_\alpha(T)$ (open symbols) and $\tau_{2R_g}(T)$ (filled symbols). Solid, dotted, and dashed lines are fit to the data at density $\rho = 1.0, 0.85$, and 0.7 : the data is fitted using relation $D \sim \tau_\alpha^{-\xi}$ for the monomers and using $D \sim \tau_{2R_g}^{-\xi}$ for the molecules.

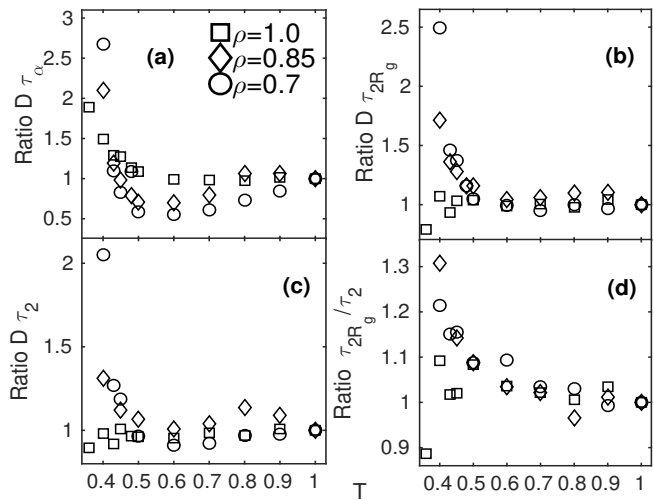


Figure 6. Ratios of (a) $D\tau_\alpha$, (b) $D\tau_{2R_g}$, (c) $D\tau_2$, and (d) τ_{2R_g}/τ_2 are plotted against temperature T . The ratios are defined as $D\tau(T)/D\tau(T = 1.0)$.

decreasing below $T = 1.0$, which again start increasing from $T = 0.5$ and reach a value around 2.1 and 2.7 respectively at the lowest temperature $T = 0.4$ of the density $\rho = 0.85$ and $\rho = 0.7$. In the higher density system, the SE ratio remains constant up to $T = 0.6$, which start increasing from $T = 0.5$ and attains a value around 2.0 at the lowest temperature $T = 0.36$. Below temperature $T = 0.5$, where fractional SE relation is found at all three densities (see Fig. 5), the SE ratio also start increasing. A higher value of the SE ratio correlates with the smaller value of the fractional SE exponent ξ . Thus, we show that the SE relation breaks down in the supercooled linear polymer melt for all three densities.

Polymer chains in this study are flexible, which show

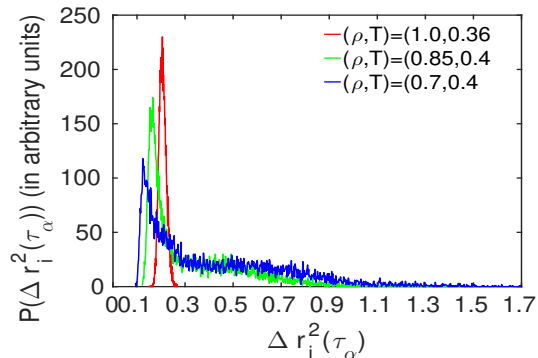


Figure 7. Probability distribution of squared displacements of monomers, $P(\Delta r_i^2(\tau_\alpha))$ at $t = \tau_\alpha$.

large shape fluctuations. Therefore, it is compelling to examine the violations of the SE relation at the molecular level. Diffusion constant D is plotted against molecular relaxation in Fig. 5, where data is fitted using the relation $D \sim \tau_{2R_g}^{-\xi}$. Here, relaxation time τ_{2R_g} is computed at wave vector $k = 2\pi/2R_g$; R_g is the average radius of gyration of the chains. Variation in τ_{2R_g} with temperature is shown in Fig. S6 of the SM [50]. The value of the exponent ξ is 1.0 from $T = 2.0 - 0.6$ for both lower density systems. However, in the supercooled regime ($T = 0.5 - 0.4$), the value of the exponent are $\xi = 0.91$ and 0.83 respectively for the density $\rho = 0.85$ and $\rho = 0.7$, thus, show a weak (exponent ξ closer to unity) violation of molecular SE relation; the degree of violation is more at $\rho = 0.7$. On the other hand, $\xi = 1.0$ for whole temperature range (of this study) at higher density, thus, D and τ_{2R_g} are coupled at this density. We examine the SE ratio of $D\tau_{2R_g}$ also in all three systems and found that in the temperature range where $D \sim \tau_{2R_g}^{-\xi}$ is fractional, the SE ratio also starts increasing from the value 1.0 and reach a value around 1.65 and 2.5 respectively for $\rho = 0.85$ and $\rho = 0.7$ (see Fig. 6(b)). However, in the higher density system, this ratio oscillates around 1.0. Thus, this study shows the violation of the molecular SE relation only in the lower density systems, whereas the violation of monomer SE relation is seen at all three densities. Many investigations show a role of mobile and immobile species and jump like motions for the violations of the SE relation, therefore next we look for many possible origins of violations of SE relations in this unentangled flexible polymer melt.

D. Distribution of particles' mobility and jump like motion

In order to identify jump like motion of monomers, we compute the distribution of average squared displacement, $\Delta r_i^2(\tau_\alpha) = |\mathbf{r}_i(\tau_\alpha) - \mathbf{r}_i(0)|^2$ of individual monomers and its probability distribution. Fig. 7 shows

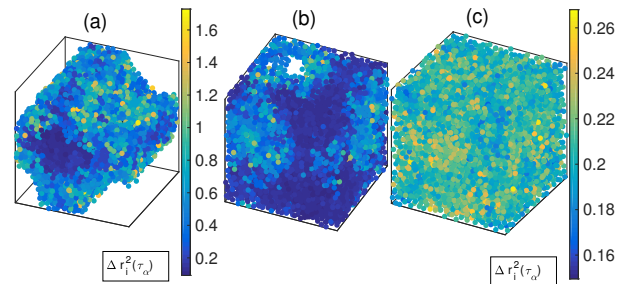


Figure 8. Mean squared displacements per monomer at $t = \tau_\alpha$ of (a) density $\rho = 0.7$ at $T = 0.4$, (b) density $\rho = 0.85$ at $T = 0.4$, and (c) density $\rho = 1.0$ at $T = 0.36$. Left color bar is for (a) and (b), whereas right color bar is for (c).

that $\Delta r_i^2(\tau_\alpha)$ ranges as $0.10 - 1.7$ and $0.13 - 1.5$ for $\rho = 0.7$ and 0.85 at $T = 0.4$, whereas $\Delta r_i^2(\tau_\alpha)$ varies as $0.15 - 0.265$ at $T = 0.36$ for the higher density. We examine the distribution of the squared displacement at $t = \tau_\alpha$ because it corresponds to the average cage relaxation time. In both lower density systems at $T = 0.4$ (see Fig. 8(a-b)), the monomers near the cavities have larger displacements, whereas the monomers in the core have smaller displacements (the monomers of the core start freezing, whereas the monomers near the cavities are still in the gaseous phase) at $t = \tau_\alpha$, which creates a disparity in their displacements resulting in the pronounced dynamic heterogeneity [56] in both lower density systems. The dynamic heterogeneity is less pronounced in $\rho = 0.85$ system than the $\rho = 0.7$ system because of a narrower distribution of displacements as the surface of the cavities reduces. This analysis suggests that the extent of the dynamic heterogeneity in the monomer motion of both lower densities arises due to a large disparity in their displacements because of the presence of surfaces around the cavities [57]. Thus, it shows that the disparity in the motion of the particles due to the jump-like motion and caging, causes violation of the SE relations in polymer systems similar results are found in the studies on other glass formers [10, 12]. Now, it is interesting to look at the characterization of dynamic cages from the analysis of single particle motion.

To understand single particle motion, we look into self part of the van-Hove correlation function $G_s(\mathbf{r}, t)$ [1],

$$G_s(\mathbf{r}, t) = \frac{1}{N} \left\langle \sum_{i=1}^N \delta(\mathbf{r} + \mathbf{r}_i(0) - \mathbf{r}_i(t)) \right\rangle. \quad (7)$$

to identify the transient cages formed in the systems near the glass transition. Fig. 9 shows a plot of $4\pi r^2 G_s(r, t)$ vs r of monomers at temperature $T = 0.4$ and $T = 0.36$, where the cages are more pronounced as evidenced from the $F_s(k, t)$. State points at one higher and two lower densities are compared and analyzed at time scales, $t = 0.5\tau_\alpha$, τ_α , $2\tau_\alpha$, $4\tau_\alpha$, and $10\tau_\alpha$. In Fig. 9(a), $G_s(r, t)$ of higher and lower density systems are compared at $T = 0.4$, which shows that both lower density systems exhibit a peak at smaller r and a small hump around $r \sim 1.0$

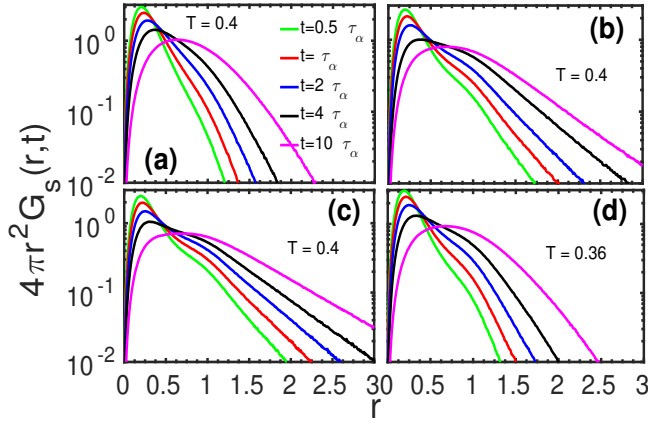


Figure 9. $4\pi r^2 G_s(r, t)$ of monomers is plotted against radial distance r at times $t = 0.5\tau_\alpha, \tau_\alpha, 2.0\tau_\alpha, 4.0\tau_\alpha,$ and $10.0\tau_\alpha$. (a) $\rho = 1.0$, (b) $\rho = 0.85$, (c) $\rho = 0.7$, and (d) $\rho = 1.0$.

($= \sigma$) at $t = 0.5\tau_\alpha, \tau_\alpha, 2\tau_\alpha,$ and $4\tau_\alpha$. The first peak in the $G_s(r, t)$ is due to the caging of the monomers. However, the hump in both lower density systems at $T = 0.4$, is due to hopping of the particles from the transient cages (see Fig. 7, Fig. 8(a)&(b)); similar humps are reported by Lam [58] in polymer melts at low temperatures.

At $T = 0.4$, a weak hump is present in the $G_s(r, t)$ of the higher density system, therefore, it shows less heterogeneous dynamics that has faster relaxation than both lower density systems (see Fig. 4(a)). In contrast, $G_s(r, t)$ shows a smaller hump at $t = 0.5\tau_\alpha, \tau_\alpha, 2\tau_\alpha,$ and $4\tau_\alpha$ at $T = 0.36$ of the higher density system, similar to both lower densities (see Fig. 9(b)). Interestingly, the relaxation dynamics of the higher density system at $T = 0.36$ also becomes nearly comparable to $T = 0.4$ of both lower density systems (see Fig. 4(a)) where relaxation dynamics of these systems are also comparable. Thus, this system shows transient monomer cages at all densities near the glass transition temperature T_c .

In the supercooled regime, due to the presence of molecular cages, these molecules undergo a large directed displacements by translation to escape from the self-generated barriers, thus relaxing the accumulation of the stress due to hindered motion. To identify such motions, we plot typical trajectories of the displacements of the randomly selected single monomers $|\mathbf{r}_i(t) - \mathbf{r}_i(0)|$ against time t at the lowest temperatures $T = 0.4$ and 0.36 to see whether there are large displacements in the monomers. Fig. 10(a-c) show the typical trajectories of $\rho = 0.7$ and 0.85 system at $T = 0.4$, and $\rho = 1.0$ system at $T = 0.36$. These trajectories show the intermittent large displacements in the motion of monomers that have deviations from the regular random walk. Jump like motions are difficult to identify in polymer systems with longer chains. An earlier study using continuous time random walk on shorter chains ($n = 4$) identifies jumps in the supercooled linear polymer melt [37]. However, jump like motions are found in several studies of glass-forming binary Lennard-Jones systems (see Refs. [59, 60]). These intermittent

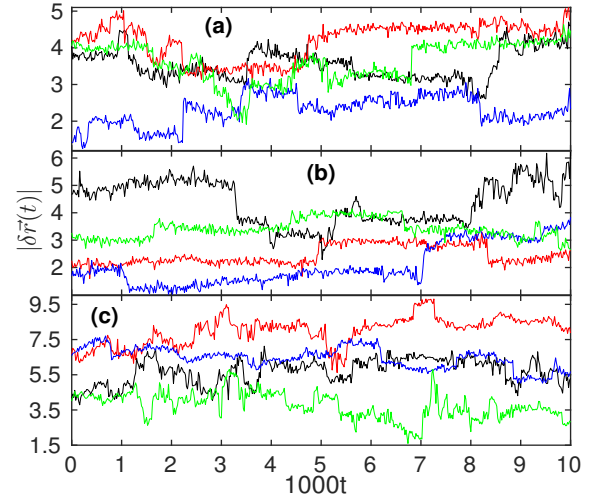


Figure 10. Trajectories of the monomer displacements, $|\delta\vec{r}(t)| = |\vec{r}_i(t) - \vec{r}_i(0)|$ for (a) $\rho = 1.0$ at $T = 0.36$, (b) $\rho = 0.85$ at $T = 0.4$, (c) $\rho = 0.7$ at $T = 0.4$. Different colors in (a), (b), and (c) correspond to the randomly selected monomers of different polymer chains.

large displacements of the monomers are related to the fluctuations in the molecular configurations, which appear at the same state points where the violation of the SE relation is much pronounced, *i.e.*, at $T = 0.4$ and 0.36 for the lower density and higher density systems, respectively.

E. Violation of Stokes-Einstein-Debye relations

Polymers are extended macromolecules that have rotational degrees of freedom along with translational ones. The average rotational motion of the polymer molecules can be quantified from the rotation of the unit vector along the end-to-end vector. The relaxation time of the rotational motion can be calculated as $\tau_l = \int_0^\infty C_l^r(t) dt$, where $C_l^r(t) = \langle P_l(\cos \theta(t)) \rangle$ is the l^{th} order rotational correlation function of the non-spherical molecules [28]. Here, $\cos \theta(t) = \hat{\mathbf{e}}(0) \cdot \hat{\mathbf{e}}(t)$, and $\hat{\mathbf{e}}(t)$ is a unit vector along the end-to-end vector $\mathbf{e}(t) = \mathbf{r}_1(t) - \mathbf{r}_n(t)$ of a polymer chain; $P_l(\cos \theta(t))$ is the Legendre polynomial of order l . Molecular liquids show translation-rotation coupling at high temperatures and obey the relation $D\tau_l = \text{constant}$, which means that $D \propto \tau_l^{-1}$. Many studies show that near the glass transition the translation-rotation relaxation dynamics is decoupled [33, 34]. The failure of SED relation is usual in the molecular liquids [61], which is much more pronounced in the orientational glasses for *e.g.* see Refs. [33, 62]. The polymer model we used in this study is a non-polar, therefore, we use orientational relaxation time, especially, τ_2 due to up-down symmetry, to examine the SED violation [15, 63]; the data is fitted to the relation $D \sim \tau_2^{-\xi}$ in Fig. 11, and the variation of τ_2 with temperature is shown in Fig. S6 of the SM

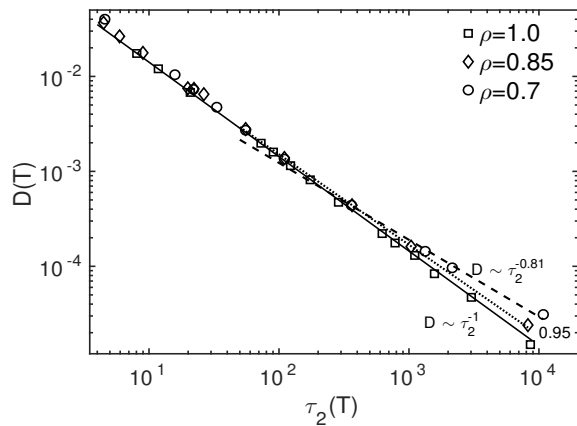


Figure 11. Diffusion coefficient $D(T)$ is plotted against $\tau_2(T)$. Solid, dotted, and dashed lines are fit to the data at density $\rho = 1.0$, 0.85 , and 0.7 , respectively. The data is fitted using relation $D \sim \tau_2^{-\xi}$.

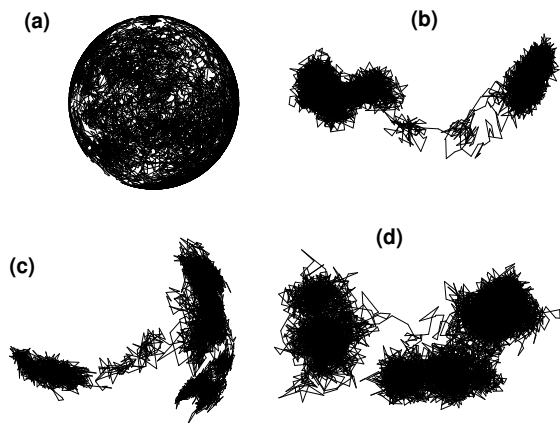


Figure 12. The trajectory of the unit vector along an end-to-end vector of a randomly selected chain of the system for the time interval $\delta t = 2500$. (a) $\rho = 0.85$ at $T = 1.0$, (b) $\rho = 0.85$ at $T = 0.4$, (c) $\rho = 1.0$ at $T = 0.4$, and (d) $\rho = 1.0$ at $T = 0.36$.

[50]. Recently, dependency of SED relation on the degree of Legendre polynomial, l is examined by Kawasaki and Kim in supercooled water [64]. In both lower density systems, exponent $\xi = 1.0$ from $T = 2.0$ to 0.6 , whereas in the supercooled regime ($T = 0.5$ to 0.4), the exponent $\xi = 0.95$ and $\xi = 0.81$, respectively for $\rho = 0.85$ and $\rho = 0.7$ system. Thus shows a weak decoupling in D and τ_2 near T_c in both lower density systems, which is significant in the $\rho = 0.7$ system. On the other hand, in the higher density system, $\xi = 1.0$ from high to low temperatures (up to $T = 0.36$), which means that D and τ_2 are coupled even near the T_c .

Analogous to the ratios of predictors of SE relation, we compute ratio of $D\tau_2 = \text{constant}$ as a predictor for the SED violation [29]. The value of $D\tau_2$ is scaled with its value at temperature $T = 1.0$, which is shown in Fig. 6(c) (ratio is defined as $D\tau_2(T)/D\tau_2(T = 1.0)$). In both lower density systems, this ratio starts from 1.0 and fluctuates

around this value from $T = 0.9$ to $T = 0.6$. It starts increasing from $T = 0.5$ and reaches around values 1.3 and 2.0 (at $T = 0.4$) for $\rho = 0.85$ and $\rho = 0.7$ systems, respectively. This shows that SED relation is very weakly violated in $\rho = 0.85$ system, similar to the molecular SE violations, whereas violation is more for the $\rho = 0.7$ system. In the temperature range where there is a maximum value of SED ratio, the exponent ξ reduces, thus shows a correlation between them. In the higher density system, the SED ratio fluctuates close to 1.0 except at the lowest temperature $T = 0.36$, where ratios has value around 0.8. This implies that SED relation is valid in the higher density system even near T_c . Further, the translation-rotation decoupling is examined by the ratio of center of mass density relaxation time from $F_s^C(k, t)$ to rotational relaxation time as τ_{2R_g}/τ_2 scaled with its value at temperature $T = 1.0$ (see Fig. 6(d)). Similar to the ratio for $D\tau_2$, the ratio for τ_{2R_g}/τ_2 and $D\tau_{2R_g}$ also oscillate around 1.0 (all these values are scaled with corresponding value at $T = 1.0$), which means that translational molecular relaxation time and rotational relaxation time are coupled in the higher density system. However, the ratio for τ_{2R_g}/τ_2 starts increasing from $T = 0.9$ and reaches around the values 1.3 and 1.2 respectively for $\rho = 0.85$ and $\rho = 0.7$ at the low temperature $T = 0.4$. This shows a very weak decoupling between τ_{2R_g} and τ_2 in both lower density systems. Such decoupling was also found in an experiment by Edmond *et al.* [16] in the glass transition of a colloidal system, and in a simulation study of glassy dumbbells [33]. We expect a strong violation of SE and SED relations in these systems, if the observed trend is continued below T_c .

As many studies show that the violation of SED relation is attributed to the enhanced hopping process in the rotational motion [36]. Therefore, we look into the typical trajectory of an orientation vector $\hat{e}(t)$ over the unit sphere of few randomly selected polymer chains. In Fig. 12, we compare the rotation of $\hat{e}(t)$ of polymer chains at one high temperature and two low temperatures. At $T = 1.0$ of the density $\rho = 0.85$, the trajectory of $\hat{e}(t)$ (Fig. 12(a)) shows a random walk, which uniformly spans over the sphere. However, the higher and lower density systems at the low temperatures (see Fig. 12(b-d)), show an intermittent motion of the rotational vector, which is a bit pronounced in the lower density systems. Fig. 12(d) shows a trajectory of a randomly selected chain of the higher density system, which shows a weak confinement at $T = 0.36$. Earlier studies by Jose *et al.* show the pronounced violation of SED relation, which is related to the strong confinement in the orientation of the molecules [62, 65] that is absent in our system. As polymer molecules are nearly spherically symmetric, they require more confinement for strong violation of the SED relation.

IV. CONCLUDING REMARKS

The violations of Stokes-Einstein and Stokes-Einsteins-Debye relations are defining characteristics of the glass transition, which are explained in terms of dynamical heterogeneities arise due to jump like motions of mobile particles, and dynamical caging of immobile particles in simulations of atomistic model glass formers [17]. Another important class of glass-forming liquids are polymers that are difficult to crystallize. Direct observation of violation of SE and SED relations in simulations of model polymers are rare because of their extended shape, and the microscopic processes such as jump like motions are difficult to detect [37]. However, the indirect observation of microscopic origins of violations of SE relation is examined in the earlier studies [11, 38]. Due to extended shape of the polymers, we widen our study of the supercooled polymers near the glass transition to the lower density systems, where available volume for polymer chains is abundant, especially near the surface of the bi-continuous phase. Extensive molecular dynamics simulations of a linear Lennard-Jones polymer melt systems are performed at monomer number densities $\rho = 0.7, 0.85,$ and 1.0 from $T = 2.0$ to $T = 0.36$. For the first two densities, system form bi-continuous phase, whereas the higher density system is homogeneous near glass transition temperature T_c . Single particle density relaxation properties from the $F_s(k, t)$ at different time origins in the supercooled bi-continuous phases compared with that at $\rho = 1$ at the same temperature show that the density relaxation is independent of the time origin in the bi-continuous phases near the glass transition. The collective relaxation properties obtained from $G_d(r, t)$ shows that the bi-continuous phases are stable within our simulation time. In these systems that differ in their density, we look for direct evidence of SE violation in the density relaxation of monomer and center of mass of polymer chains, and the SED violation of the polymer chains, near their MCT glass transition temperatures.

We show that monomer SE relation is violated for all three systems in the supercooled regime, which is pronounced in both lower density systems. The pronounced violation of the SE relation in both lower density systems

is caused by the structural inhomogeneities and resulting dynamic heterogeneity due to the enhanced disparity in the monomer mobility in comparison to the higher density system. In the temperature range $T = 2.0 - 0.6$, the molecular SE relation is obeyed in the higher and both lower density systems. However, in the supercooled regime, the higher density system obeys the molecular SE relation, whereas both lower density systems weakly violate it. At the lowest temperature of all three densities, we identify a hump at $r = \sigma$ and a peak at small r in $G_s(r, t)$ that together show the monomer cages and jump like motions in the monomer movement, which was also shown in the earlier studies of glass-forming binary mixtures [10, 12]. Our study further show that disparity in the mobility of the monomers caused by the structural inhomogeneities, is more in both lower density systems compared to the higher density system. Thus, we show that violations in the monomer and molecular SE relations are attributed to the presence of mobile and immobile particles, the jump like motions, and cage formation in this linear polymer melt at temperatures near T_c . We also show that the unit vector associated with the polymer chains undergoes confinement. Thus, there is weak violation in the SED relation for both lower density systems, supported by the intermittent motion found in the typical trajectory of the end-to-end unit vector. Our study also show the glass transition in the presence of static structural inhomogeneities, very much similar to the continuous phases. Many aspects of the formation of the glassy domains in the model glassy binary mixtures are studied in the simulations [47, 66] and experiments [44, 45, 67], where glass transition and phase separation coexist, though the inter-molecular potentials and molecular geometry are different than our study. Therefore, the simulations with more model potentials and varying range of attractions are required for obtaining the quantitative information about the microscopic glassy domains formed in the phase separating systems.

ACKNOWLEDGMENTS

We thank HPC facility at IIT Mandi for computational support. PPJ acknowledge financial support from SERB project no. EMR/2016/005600/IPC.

-
- [1] J. P. Hansen and I. R. McDonald, *Theory of Simple Liquids* (Academic Press, London, 2006).
 [2] G. G. Stokes, Trans. Cambridge Philos. Soc. **9**, 8 (1851).
 [3] A. Einstein, Ann. Phys. **322**, 549 (1905).
 [4] T. Kawasaki and K. Kim, Sci. Adv. **3**, e1700399 (2017).
 [5] S. Sengupta, S. Karmakar, C. Dasgupta, and S. Sastry, J. Chem. Phys. **138**, 12A548 (2013).
 [6] B. P. Bhowmik, R. Das, and S. Karmakar, J. Stat. Phys.: Theory and Expt. **07**, 074003 (2016).
 [7] Z. Shi, P. G. Debenedetti, and F. H. Stillinger, J. Chem.

- Phys. **138**, 12A526 (2013).
 [8] R. Yamamoto and A. Onuki, Phys. Rev. Lett. **81**, 4915 (1998).
 [9] In liquids at high temperatures, intermediate incoherent scattering function can be given as $F_s(k, t) = \exp(-Dk^2t) \equiv \exp(-t/\tau)$ [1], here, k is a wave vector near the first peak of static structure factor $S(k)$. This suggests that $Dk^2\tau = \text{constant}$, or $D\tau = \text{constant}$, implies that $D \propto 1/\tau$, which according to $D\eta/T = \text{constant}$, entails that $\tau \propto \eta/T$.

- [10] S. R. Becker, P. H. Poole, and F. W. Starr, *Phys. Rev. Lett.* **97**, 055901 (2006).
- [11] F. Puosi and D. Leporini, *J. Chem. Phys.* **136**, 211101 (2012).
- [12] S. Pan, Z. W. Wu, W. H. Wang, M. Z. Li, and L. Xu, *Sci. Rep.* **7**, 39938 (2017).
- [13] C. K. Mishra and R. Ganapathy, *Phys. Rev. Lett.* **114**, 198302 (2015).
- [14] M. D. Ediger, *Ann. Rev. Phys. Chem.* **51**, 99 (2000).
- [15] L. Andreozzi, A. D. Schino, M. Giordano, and D. Leporini, *J. Phys.: Condens. Matter* **8**, 9605 (1996).
- [16] K. V. Edmond, M. T. Elsesser, G. L. Hunter, D. J. Pine, and E. R. Weeks, *Proc. Natl. Acad. Sci.* **109**, 17891 (2012).
- [17] L. Berthier, G. Biroli, J. Bouchaud, L. Cipelletti, and W. Saarloos, eds., *Dynamical Heterogeneities in Glasses, Colloids and Granular Media* (Oxford University Press, New York, 2011).
- [18] E. Flenner, H. Staley, and G. Szamel, *Phys. Rev. Lett.* **112**, 097801 (2014).
- [19] C. Donati, S. C. Glotzer, P. H. Poole, W. Kob, and S. J. Plimpton, *Phys. Rev. E* **60**, 3107 (1999).
- [20] S. C. Glotzer, *J. Non-Cryst. Solids* **274**, 342 (2000).
- [21] R. Richert, *J. Phys.: Condens. Matter* **14** (2002).
- [22] W. Kob, C. Donati, S. J. Plimpton, P. H. Poole, and S. C. Glotzer, *Phys. Rev. Lett.* **79**, 2827 (1997).
- [23] P. Charbonneau, Y. Jin, G. Parisi, and F. Zamponi, *Proc. Natl. Acad. Sci.* **111**, 15025 (2014).
- [24] S.-H. Chong, *Phys. Rev. E* **78**, 041501 (2008).
- [25] Q.-Z. Zou, Z.-W. Li, Y.-L. Zhu, and Z.-Y. Sun, *Soft Matter* **15**, 3343 (2019).
- [26] S. K. Kumar, G. Szamel, and J. F. Douglas, *J. Chem. Phys.* **124**, 214501 (2006).
- [27] P. Debye, *Polar Molecules* (Dover Publications, New York, 1929) p. 72.
- [28] B. J. Berne and R. Pecora, *Dynamic Light Scattering: With applications to Chemistry, Biology and Physics* (Dover Publications, New York, 2000).
- [29] G. Tarjus and D. Kivelson, *J. Chem. Phys.* **103**, 3071 (1995).
- [30] M. G. Mazza, N. Giovambattista, H. E. Stanley, and F. W. Starr, *Phys. Rev. E* **76**, 031203 (2007).
- [31] K. L. Ngai, *Phil. Mag. B* **79**, 1783 (1999).
- [32] P. G. de Gennes, *Scaling Concepts in Polymer Physics* (Cornell University Press, Ithaca and London, 1979).
- [33] S.-H. Chong and W. Kob, *Phys. Rev. Lett.* **102**, 025702 (2009).
- [34] F. H. Stillinger and J. A. Hodgdon, *Phys. Rev. E* **50**, 2064 (1994).
- [35] C. D. Michele and D. Leporini, *Phys. Rev. E* **63**, 036701 (2001).
- [36] C. D. Michele and D. Leporini, *Phys. Rev. E* **63**, 036702 (2001).
- [37] J. Helfferich, F. Ziebert, S. Frey, H. Meyer, J. Farago, A. Blumen, and J. Baschnagel, *Phys. Rev. E* **89**, 042603 (2014).
- [38] F. Puosi, A. Pasturel, N. Jakse, and D. Leporini, *J. Chem. Phys.* **148**, 131102 (2018).
- [39] C. Balbuena and E. R. Soulé, *J. Phys.: Condens. Matter* **32**, 045401 (2020).
- [40] F. W. Starr, S. Sastry, J. F. Douglas, and S. C. Glotzer, *Phys. Rev. Lett.* **89**, 125501 (2002).
- [41] C. Bennemann, W. Paul, K. Binder, and B. Dünweg, *Phys. Rev. E* **57**, 843 (1998).
- [42] K. Huang, *Introduction to Statistical Physics* (CRC Press, Taylor & Francis Group, Boca Raton, FL, 2010).
- [43] G. Foffi, C. D. Michele, F. Sciortino, and P. Tartaglia, *J. Chem. Phys.* **122**, 224903 (2005).
- [44] F. Cardinaux, T. Gibaud, A. Stradner, and P. Schurtenberge, *Phys. Rev. Lett.* **99**, 118301 (2007).
- [45] P. D. Godfrin, P. Falus, L. Porcar, K. Hong, S. D. Hudson, N. J. Wagner, and Y. Liu, *Soft Matter* **14**, 8570 (2018).
- [46] P. Chaudhuri and J. Horbach, *Phys. Rev. B* **94**, 094203 (2016).
- [47] V. Testard, L. Berthier, and W. Kob, *Phys. Rev. Lett.* **106**, 125702 (2011).
- [48] G. S. Grest and K. Kremer, *Phys. Rev. A* **33**, 3628 (1986).
- [49] M. P. Allen and D. J. Tildesley, *Computer simulation of liquids* (Clarendon Press, Oxford, 1987).
- [50] See Supplementary Material for the details of average local packing, monomer MSD, orientational correlations functions, and relaxation times fitting.
- [51] W. Kob and J.-L. Barrat, *Phys. Rev. Lett.* **78**, 4581 (1997).
- [52] J.-L. Barrat, J. Baschnagel, and A. Lyulin, *Soft Matter* **6**, 3430 (2010).
- [53] S.-H. Chong and M. Fuchs, *Phys. Rev. Lett.* **88**, 185702 (2002).
- [54] C. A. Angel, *Science* **267**, 1924 (1995).
- [55] Y.-W. Li, C. K. Mishra, Z.-Y. Sun, K. Zhao, T. G. Mason, R. Ganapathy, and M. P. Ciamarra, *Proc. Natl. Acad. Sci.* **116**, 22977–22982 (2019).
- [56] C. P. Royall and S. R. Williams, *Phys. Rep.* **560**, 1 (2015).
- [57] J. Singh and P. P. Jose, *AIP Conf. Proc.* **2115**, 030236 (2019).
- [58] C.-H. Lam, *J. Chem. Phys.* **146**, 244906 (2017).
- [59] L. Berthier and G. Biroli, *Rev. Mod. Phys.* **83**, 587 (2011).
- [60] S. Bhattacharyya and B. Bagchi, *Phys. Rev. Lett.* **89**, 025504 (2002).
- [61] D. A. Turton and K. Wynne, *J. Phys. Chem. B* **118**, 4600 (2014).
- [62] P. P. Jose, D. Chakrabarti, and B. Bagchi, *Phys. Rev. E* **73**, 031705 (2006).
- [63] P. J. Griffin, J. R. Sangoro, Y. Wang, A. P. Holt, V. N. Novikov, A. P. Sokolov, Z. Wojnarowska, M. Paluch, and F. Kremer, *Soft Matter* **9**, 10373 (2013).
- [64] T. Kawasaki and K. Kim, *Nat. Comm.* **9**, 8118 (2019).
- [65] P. P. Jose, D. Chakrabarti, and B. Bagchi, *Phys. Rev. E* **71**, 030701(R) (2005).
- [66] A. Varughese and P. P. Jose, *J. Phys.: Conf. Ser.* **759**, 012019 (2016).
- [67] H. Tanaka, T. Araki, T. Koyama, and Y. Nishikawa, *J. Phys.: Condens. Matter* **17**, S3195 (2005).
- [68] M. Doi and S. F. Edwards, *The theory of polymer dynamics* (Clarendon Press, Oxford, 1986).

Violation of Stokes-Einstein and Stokes-Einstein-Debye relations in a supercooled polymer melt

Supplemental Material

Jalim Singh and Prasanth P. Jose*

School of Basic Sciences, Indian Institute of Technology Mandi, Kamand, Himachal Pradesh 175005, India

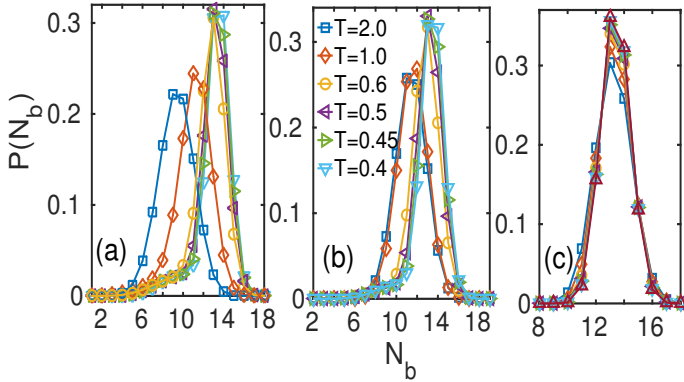


Figure S1. Average probability distribution $P(N_b)$ is plotted against N_b at $T = 2.0 - 0.36$: (a) $\rho = 0.7$, (b) $\rho = 0.85$, and (c) $\rho = 1.0$. In (a) and (b), $P(N_b)$ shows nonzero values for the smaller N_b , which corresponds to the gas-liquid phase coexistence at high temperatures. The liquid phase becomes amorphous solid-like coexisting with the gaseous particles at low temperatures.

I. LOCAL PACKING OF MONOMERS

Fig. 8 of the paper and our previous study of this system [57] show that lower density systems phase separate at low temperatures. In order to examine a variation of the local density with temperature in the phase separating systems, we calculate local packing of the monomers in the linear polymer melt system at three different densities. The local packing is obtained from the calculation of number of nearest neighbors N_b of each monomer in the first coordination shell (FCS), which is at $0 < r \leq r_{fcs}$; $r_{fcs} = 1.5$ is a position of the first minima of the radial distribution function of the system [57]. Using this FCS radius, its volume can be calculated as $V_{fcs} = (4/3)\pi r_{fcs}^3 = 14.137$, which subsequently gives the local density $\rho_l = (N_b + 1)/V_{fcs}$. Fig. S1 shows that range of N_b is 3 – 18 at $T = 0.4$ for $\rho = 0.7$ and 0.85, whereas $N_b = 9 - 18$ at $T = 0.36$ of the higher density system. Thus, the local density range is calculated as $\rho_l = 0.283 - 1.344$ at $T = 0.4$ of the lower densities $\rho = 0.7$ and 0.85, and $\rho_l = 0.707 - 1.344$ at $T = 0.36$ of the higher density system. This shows the coexistence of gas and the dense amorphous domains in both lower density systems at temperatures near T_c .

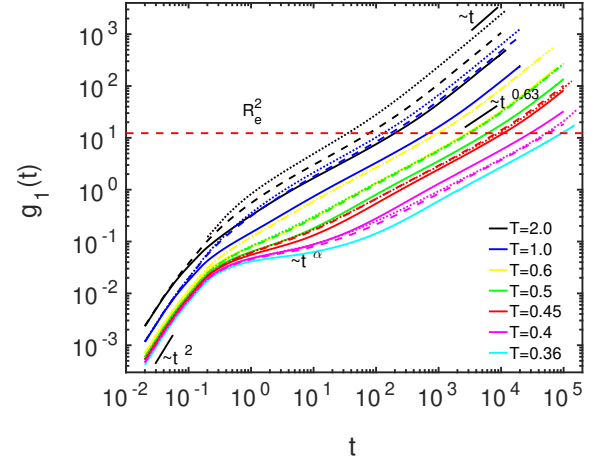


Figure S2. Mean squared displacement of monomers are plotted against time t . Solid, dashed, and dotted lines are correspond to the density $\rho = 1.0, 0.85$, and 0.7 respectively.

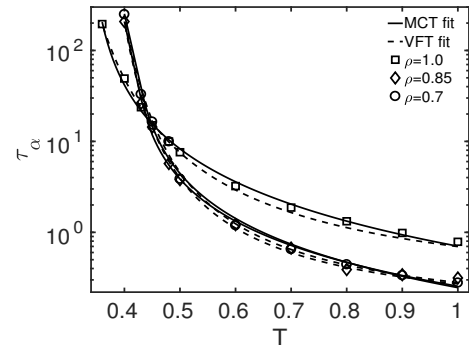


Figure S3. Fitting of α -relaxation time with MCT and VFT relations. Note that the VFT fit is a good fit to the data.

The nearest neighbor distribution averaged over the steady state configurations (see Fig. S1(c)) shows that the higher density system does not show macroscopic cavities, whereas both lower density systems show cavities as temperature reduces, resulting in the structural inhomogeneities [57]. Packing of the monomers that are inside the dense domains are similar for all three densities because of the monomers within the dense domains in both lower density systems have the same range of N_b to that the higher density system (see Fig. S1). In both lower

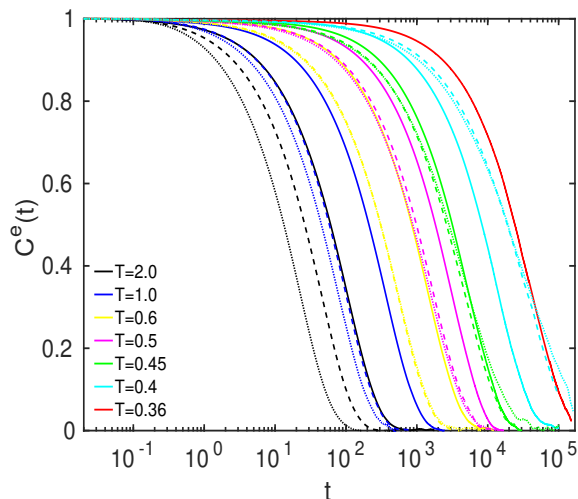


Figure S4. End-to-end vector time correlation function of polymer chains. Solid, dashed, and dotted lines are corresponding to $\rho = 1.0, 0.85$, and 0.7 .

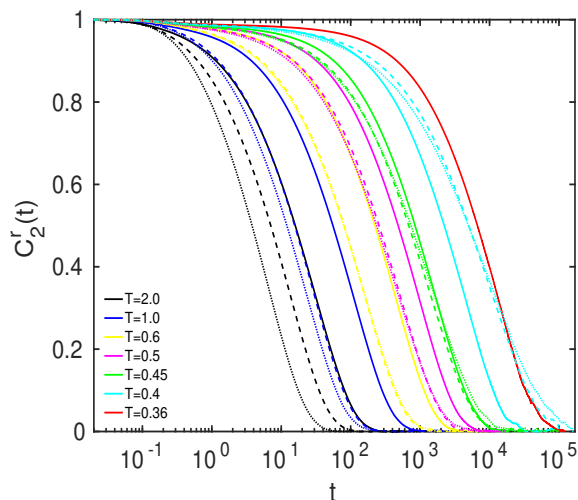


Figure S5. Relaxation of second order time correlation function of the rotational vector of polymer chains. Solid, dashed, and dotted lines are corresponding to $\rho = 1.0, 0.85$, and 0.7 .

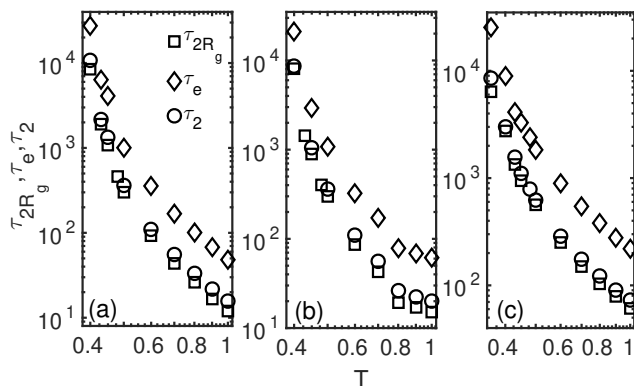


Figure S6. Molecular relaxation times τ_{2Rg} , τ_e , and τ_2 are plotted against temperature T at density (a) $\rho = 0.7$, (b) $\rho = 0.85$, and (c) $\rho = 1.0$.

densities (see Fig. S1(a) and Fig. S1(b)), the major peak of $P(N_b)$ shifts to $N_b = 13$ and 14 at low temperatures, whereas in the higher density system (see Fig. S1(c)), the peak height grows at $N_b = 13$ and 14 from high to low temperatures. At low temperatures, a hump in $P(N_b)$ at $N_b \simeq 8-10$ is appearing in both lower density systems, which is absent in the higher density system. This hump in $P(N_b)$ confirms the structural inhomogeneity in both lower density systems, however an approximately equal peak height at $N_b = 13$ and 14 indicates the similarity in the local packing of the glassy domains in all three systems at low temperatures.

II. RELAXATION TIME AND THE FITTING

The monomer α -relaxation times are plotted against temperature T in Fig. S3 at three different densities. The τ_α vs T curves are fitted with the MCT and VFT relations, as described in the main text. The α -relaxation time is longer for the higher density system compared to the both lower density systems up to $T = 0.45$. At $T = 0.4$, the α -relaxation time of the both lower densities show a crossover to the higher density system, which is also evident in the $F_s(k, t)$ of the main text.

III. TRANSLATION

An average displacement of a particle from its initial position can be calculated from its mean-squared displacement (MSD) $g_1(t)$,

$$g_1(t) = \langle (\mathbf{r}(0) - \mathbf{r}(t))^2 \rangle, \quad (\text{S1})$$

which is shown in the Fig. S2(a) at various temperatures of the three different densities. Fig. S2(a) shows that monomers show ballistic motion ($\sim t^2$) at short time, crossing over to the intermediate caging regime ($\sim t^\alpha$, $0 < \alpha < 1$) owing to various interactions, bonding as well as non-bonding type. There exists a ballistic regime in the MSD of monomers followed by the caging regime, which is due to the chain hindrance as that varies with power law $g_1(t) \sim t^{0.63}$ [52]. Finally, the diffusive regime in the monomer MSD starts from time $t \sim 10^3$ at the temperature $T = 2.0$, whereas at lowest temperatures ($T = 0.4$ and $T = 0.36$) the diffusive regime starts at the time scale of $t \sim 10^6$ [52]. Fig. S2(a) shows that as the temperature get lowered the caging of the monomer MSDs becomes more pronounced, which is supported by the $F_s(k, t)$ shown in main text. The monomer MSD of the higher density system is slower than the both lower density systems above $T = 0.4$, which shows a crossover at $T = 0.4$, where the monomer MSD of both lower density systems slows down.

IV. ORIENTATION

Further understanding of the molecular relaxation is obtained from the rotational motion of the polymer chains. An autocorrelation function of the End-to-end vector is defined as [68]

$$C^e(t) = \frac{\langle \mathbf{e}(0) \cdot \mathbf{e}(t) \rangle}{\langle \mathbf{e}(0) \cdot \mathbf{e}(0) \rangle}, \quad (\text{S2})$$

which gives detail of the molecular shape relaxation of the polymers. Fig. S4(a) shows the $C^e(t)$ of polymer chains at different temperatures of three densities. The relaxation of $C^e(t)$ is slower with increase in density at temperatures $T = 2.0$ and 1.0 . Below these temperatures, the relaxation of $C^e(t)$ becomes identical for both lower densities. However, $C^e(t)$ of the higher density system decays slower than both lower density systems up to $T = 0.45$. A crossover in the relaxation time of both lower density appears at $T = 0.4$, $C^e(t)$ relax very slowly. We have computed the time constant for end-to-end vector relaxation at all temperatures, which is defined as $\tau_e = \int_0^\infty C^e(t) dt$. A variation in τ_e with T is plotted in Fig. S6 at three different densities, which is qualitatively similar to the $C^e(t)$. The relaxation of $C^e(t)$ has contributions from the rotation as well as shape fluctuations of the polymer chains, thus we compute rotational correlation functions.

The rotational relaxation time is quantified from the rotational correlation function $C_l^r(t)$ for a non-spherical molecule [28]. Hydrodynamic SED model of rotational

relaxation predicts an exponential relaxation of $C_l^r(t)$, *i.e.*, $C_l^r(t) = e^{-t/\tau_l}$ for liquids at high temperatures, where τ_l is the time constant of l^{th} order orientational correlation function. The rotational correlation functions corresponding to $l = 2$, *i.e.*, $C_2^r(t)$ is plotted in the Fig. S5. The effect of density on the nature of the relaxation of $C_2^r(t)$ is similar to the $C^e(t)$, as described above. At high temperatures, $C_2^r(t)$ shows exponential relaxation as predicted by the SED model. However, at temperatures ($T = 0.45 - 0.4$), $C_2^r(t)$ not only slows down but also shows an emergence of a shoulder, immediately after the fast initial decay. The appearance of the shoulder hints formation of cages in the rotational motion of the polymer molecules due to the orientational confinement at small angles. These small angle confinements are correlated to the confinement of rotational motion, shown in the trajectory of the unit vectors (see Fig. 12 of the main text).

A comparison of variation in translational molecular relaxation time τ_{2R_g} , end-to-end vector relaxation time τ_e , and rotational relaxation times τ_2 with temperature and density, is shown in Fig. S6. All these relaxation times grow as temperature reduces for all three density systems, though they are higher for the higher density system up to $T = 0.45$. A crossover in the relaxation times is also observed around $T = 0.4$ for both lower density systems. Interestingly, these relaxation time at $T = 0.36$ of the higher density system, reach near to the value at $T = 0.4$ of both lower density systems.